

A Comparison **between** the TOPEX/POSEIDON Data and  
a Global Ocean General **Circulation** Model **during** 1992-93

Yi Chao and Lee-Lueng Fu

Jet Propulsion Laboratory, California institute of Technology

4800 Oak Grove Drive, Pasadena, California 91109-8099

(Tel: 818-354-8168; Fax: 81 8-393-6720; H-mail: [yc@cox.jpl.nasa.gov](mailto:yc@cox.jpl.nasa.gov))

(submitted for publication **in** the second special TOPEX/POSEIDON issue of  
Journal of Geophysical Research, February 1995, revised July 1995)

## Abstract

The TOPEX/POSEIDON altimetric sea level observation during 1992-93 was used to validate the simulation made by a global ocean general circulation model (OGCM) forced by the daily wind stress and heat flux derived from the National Meteorological Center operational analysis. The OGCM is a version of the Modular Ocean Model with a horizontal resolution of 2 degrees in longitude and 1 degree in latitude and 22 levels in the vertical. The model simulation is compared to the observation at spatial scales on the order of 500 km and larger. Only the temporal variations are examined. The variability is composed primarily of the annual cycle and intraseasonal fluctuations (periods shorter than 100 days). The basic features of the annual cycle are simulated well by the model. Major discrepancies are found in the eastern tropical Pacific, as well as the eastern North Pacific and most of the interior of the North Atlantic. The culprit is suspected to be the inadequate heat forcing and mixing parameterizations of the model. Significant intraseasonal variability is found in the central North Pacific and the Southern Ocean. The simulation is highly correlated with the observation at periods from 20 to 100 days. The spatial scales are larger than 1000 km in many places. These variabilities are apparently the barotropic response of the ocean to wind forcing. The results of the study provide a basis for future assimilation of the data into the OGCM for improved description of the large-scale ocean variabilities.

The progress in understanding the ocean circulation strongly depends on the availability of oceanic observations, which aid one in constructing numerical models capable of simulating the current ocean circulation and possibly predicting its future evolution and effects on climate. In-situ instruments (tide gauge, expendable bathythermographs, current meter moorings, and drifting buoys, etc.) generally provide sparse oceanic measurements over the world ocean, and thus, are not sufficient to depict synoptic-scale ocean variabilities over the world ocean. Satellite altimeter is able to measure the sea level of the world ocean on the order of 10 days, and therefore provides truly global data sets for ocean circulation studies. Despite its global coverage, satellite altimetry provides only two-dimensional information of the ocean surface. However, this two-dimensional information is related to the ocean interior through the dynamics and thermodynamics of the ocean. Therefore altimetry observation provides a useful boundary condition for the 3-dimensional ocean circulation (e.g., **Blayo** et al., 1994).

While it is unlikely to have global observations of the 3-dimensional state of the ocean with sufficient sampling for climate studies, using a model to assimilate incomplete observations is a viable approach to the description of the ocean. In the past, the assimilation of altimeter data is mainly confined to regional models (see **Ghil** and **Malanotte-Rizzoli**, 1991, for a review). A future goal of our research is to assimilate the altimeter data into a global primitive-equation ocean general circulation model (**OGCM**) for describing the 3-dimensional flow and density fields of the ocean. As a first step toward such an effort, the purpose of this study is to determine the skill of a global **OGCM** in simulating the sea level variability as measured by the **TOPEX/POSEIDON** altimeter. This step is essential before assimilating the altimeter data into the **OGCM**. By conducting intercomparisons between the model simulation and data, one can identify the deficiencies of the **OGCM**, and establish a basis for its future improvement. The results are also useful for developing a data assimilation system, which requires the knowledge of the model error.

The **OGCM** used in the study is the Modular Ocean Model (**MOM**) developed by NOAA's Geophysical Fluid dynamics Laboratory (**Pacanowski** et al., 1991). The model is based on the

original Bryan-Cox primitive-equation ocean model (Bryan, 1969; Cox, 1984). The Bryan-Cox model (or MOM) is the most widely used OGCM for a variety of applications in climate studies. For instance, one version of the Bryan-Cox model has been applied to the Pacific Ocean (Leetmaa and Ji, 1988), and now is the operational ocean model used at National Meteorological Center (NMC). The horizontal resolution of the model was chosen to be 2 degrees in longitude and 1 degree in latitude, resolving only the large scales of the ocean. The choice was made based on the sampling capabilities of the altimeter data. Although the altimeter resolves scales down to 6 km along its ground track, its cross-track resolution is limited by the relatively large distance between the tracks (200-300 km for TOPEX/POSEIDON). The focus of the study is thus limited to scales larger than 200-300 km.

Section 2 describes the TOPEX/POSEIDON data. Section 3 describes the model configuration, the air-sea fluxes, and the experiment design. The intercomparisons between the TOPEX/POSEIDON data and the OGCM simulation are presented in section 4 in terms of the sea level variability over the world ocean on the annual and intraseasonal time scales (defined from 20 to 100 days). Finally, section 5 presents a summary and discussions.

## 2 The TOPEX/POSEIDON data

The altimeter data used in the study were collected from the NASA dual-frequency radar altimeter and the Centre National d'Etudes Spatiales (CNES) single-frequency solid-state radar altimeter (Fu et al., 1994) during the first 360 days of the TOPEX/POSEIDON mission (September 23, 1992- September 18, 1993). Standard corrections and editing procedures were applied as suggested in the Geophysical Data Record Users Handbook (Callahan, 1993). Additional corrections were applied for the effects of the ocean tides using the model of Cartwright and Ray (1990), the solid earth tides, and the pole tide. Because of the residual tidal errors were still on the order of 5 cm, an empirical correction for the residual M2, S2, K1 and O1 tides was also applied to the data (Schrama and Ray, 1994). Additionally, the inverted barometer correction was applied to remove the sea level's static response to atmospheric pressure changes, i.e., 1 mb change of

atmospheric pressure corresponds to about -1 cm sea level change (Wunsch, 1972; Fu and Pihos, 1994). The altimeter data were first interpolated to fixed grids 6,2 km apart along each satellite track for **colinear** analysis. The time averages of sea level at each grid were then calculated and removed. To create arrays of time series on a regular space-time grid for the analysis, the sea level data were interpolated onto a space-time grid of 1 degree by 1 degree box at 3-day intervals. A Gaussian weighting function was used in both spats and time with e-folding scales of 500 km and 5 days, respectively. The resulting data set suppresses significant portions of the **mesoscale** energy, and retains mainly the large-scale sea level variabilities.

### 3 A global ocean general circulation model

As noted in the Introduction the model used in the study is based on the Modular Ocean Model (MOM). The particular model version uses a rigid-lid approximation which permits large time steps in order to reduce the computational cost. Under the rigid-lid approximation, the sea level is a diagnostic variable derived from the barotropic stream function, The model domain covers the world ocean from 80°S to 80°N with realistic geometry. The bottom topography was derived from the 1/12° by 1/12° ETOPO5 **bathymetry** data, **and** was **interpolated** to the nearest model level, The horizontal resolution is 2 **degrees** in longitude. and 1 degree in latitude. There are 22 levels in the vertical. At lateral walls, a no-slip boundary condition is applied and no flux of heat and salt is allowed. The conventional second-order operator is used for both the horizontal and vertical **subgrid-scale parameterizations**. The horizontal mixing coefficients are constant. The vertical mixing coefficients are derived from empirical relationships with the Richardson number ( $R_i$ ) according to **Pacanowski** and Philander (1981). Under this vertical mixing scheme, the vertical mixing coefficients for momentum ( $A_{MV}$ ) and tracers ( $A_{TV}$ ) are given as:

$$\begin{aligned}
 A_{MV} &= A_{MB} + \gamma/(1+\alpha R_i)^n \\
 A_{TV} &= A_{TB} + \gamma/(1+\alpha R_i)
 \end{aligned}
 \tag{1}$$

where the  $R_i$  is defined as:

$$R_i = \beta g T_z / (u_z^2 + v_z^2) \quad (2)$$

where  $A_{MB}$  ( $=0.0134 \text{ cm}^2\text{s}^{-1}$ ) and  $A_{TB}$  ( $=0.00134 \text{ cm}^2\text{s}^{-1}$ ) are the background mixing parameters, the coefficient of the thermal expansion of water  $\beta = 8.75 \times 10^{-6} (T+9)$ ,  $T$  represents the potential temperature in "C,  $u$  and  $v$  are the zonal and meridional velocity components,  $g$  is the gravitational acceleration,  $n=2$ ,  $a=5$ , and  $\gamma=50 \text{ cm}^2\text{s}^{-1}$ . This corresponds to the first-order turbulence closure scheme according to Mellor and Yamada (1982). A quadratic bottom drag formulation is also applied (Rosati and Miyakoda, 1987).

The model was first run for 10 years forced by the climatological monthly wind (Hellerman and Rosenstein, 1983). The initial condition was the Levitus (1982) January temperature and salinity distributions with zero currents. The surface temperature and salinity were relaxed back to the climatological monthly values (Levitus, 1982) with a 30-day relaxation time scale. After the 10-year spinup, the model was run from January 1992 to December 1993, which coincided with the first year of the TOPEX/POSEIDON mission. The wind stress during 1992.-93 was derived from the daily wind obtained from the NMC1000-mb analysis. A wind speed dependent drag coefficient formula was used to convert the wind to wind stress (WU, 1982). The heat flux ( $Q$ ) is based on the conventional bulk formulation, which takes into account contributions from the short-wave (SW) and long-wave radiation (LW), latent heat (LH) and sensible heat (SH) fluxes, i.e.,

$$Q = SW - LW - LH - SH \quad (3)$$

The SW and LW are based on the annual-mean values, and are assumed to be only a function of latitude (Chao and Philander, 1993; Chao et al., 1993). The LH and SH are calculated as:

$$SH = \rho C_d C_p V (T_o - T_a) \quad (4)$$

$$LH = p C_d L V [E_s(T_o) - y E_s(T_a)] (0.622/P_a) \quad (5)$$

where  $V$  is the wind speed,  $y$  is the mixing ratio,  $C_d = 0.0012$ ,  $C_p = 0.24 \text{ cal g}^{-1} \text{ }^\circ\text{C}^{-1}$ ,  $L = 595 \text{ cal g}^{-1}$ ,  $p = 0.0012 \text{ g cm}^{-3}$  and  $P_a = 1013 \text{ mb}$ . The saturation vapor pressure ( $E_s$ ) is defined as

$$E_s(T) = 10194 - 2353/T \quad (6)$$

The sea surface temperature ( $T_o$ ) is directly predicted by the OGCM, while the atmospheric surface temperature ( $T_a$ ) and mixing ratio ( $y$ ) are prescribed from the daily NMC 1000-mb analysis. No fresh-water flux is used in the current model formulation because of the lack of real-time evaporation and precipitation data sets. The OGCM-simulated sea level is saved as 3-day snapshots.

## 4 Results

### 4.1 The large-scale sea level variability

Figure 1 shows the root-mean-square variability of sea level as derived from the TOPEX/POSEIDON data and the OGCM simulation during the period of September 23, 1992-September 18, 1993. The TOPEX/POSEIDON data have been smoothed over 500 km. The OGCM grid size is on the order of 200 km. Therefore, the map represents only the sea level variabilities at very large-scales. Note that the level of variability is much lower than the one which includes the mesoscale variability (e.g., Nerem et al., 1994). The global averaged standard deviation is 3.6 cm for the TOPEX/POSEIDON data and 4.0 cm for the OGCM simulation. The OGCM simulation has slightly stronger sea level variabilities than the TOPEX/POSEIDON data. This is probably because of the 1000-mb wind used to drive the OGCM, which is generally stronger than the 10-m wind.

The 1000-mb wind is used mainly because of the uncertainties in the 10-m wind associated with the parameterization of the atmospheric planetary boundary layer (Ly et al., 1991).

[ Figure 1 near here]

From Figure 1, it is seen that the OGCM is capable of producing the basic features of the observed sea level variabilities over many parts of the world ocean. In the northern oceans, strong sea level variabilities are evident near the western boundary currents, i.e., the Gulf Stream and the Kuroshio. In the Southern Ocean, both the data and the simulation suggest much weaker sea level variabilities than its northern oceanic counterpart. Moderate sea level variabilities are only evident in areas where there are strong mean currents, i.e., the Agulhas Retroflexion (not simulated by the OGCM), the East Australian Current, the Brazil/Malvinas Confluence, and the Antarctica Circumpolar Current (ACC). In the tropical Indian Ocean, good agreement is found between the data and the simulation. However, the simulation is somewhat stronger, probably due to the 1000 mb wind forcing noted above. Strong sea level variabilities are evident in the eastern part of Bay of Bengal, south of India, off the coast of Somalia, and in the Somali Basin across the northern edge of Madagascar. In the western equatorial Pacific Ocean, strong sea level variabilities are seen in the Philippine Sea near 10°N-20°N and 120°-140°E. In the eastern equatorial Pacific, strong sea level variabilities are evident near the North Equatorial Counter Current around 5°N- 10°N.

Figure 1 has also revealed a number of discrepancies. A major one is found in the eastern tropical Pacific from 10°S to 10°N, where the OGCM simulation has significantly overestimated the observed sea level variability. This overestimation is mostly due to the excessive upwelling in the OGCM, which has been found in other similar OGCM simulations probably due to the inadequate vertical mixing parameterization (Stockdale et al., 1993). The excessive upwelling creates a strong annual cycle along the equator and 10°N that is missing from the data (see Section 4.3). Another discrepancy between the data and the simulation occurs near the Gulf Stream. The simulated sea level variability is more confined to the coastal boundary when compared with the data. The reason is mostly due to the coarse spatial resolution used in the OGCM. As a result, the simulated Gulf

Stream appears much too wide and less energetic when compared with the observation and fails to separate from the coast at Cape Hatteras. Note that the strong sea level variabilities observed in the Agulhas Retroflexion and the Brazil/Malvinas Confluence regions are not simulated by the OGCM, probably due to the model's coarse resolution that fails to create the prevailing strong nonlinearity in these regions. The simulated variability in the eastern North Pacific and most of the interior North Atlantic is generally too weak, This is believed to be caused by the model deficiency in parametering the subgrid scale processes.

#### 4.2 Spectral analysis

The temporal variability from the one year data and simulation contains sea level fluctuations on the annual and intraseasonal time scales. In order to isolate the sea level fluctuations at different frequency bands, a spectral analysis was performed. Because the forcing (the wind and heat flux) and the resulting sea level variability have a predominant latitudinal dependence, the results of the spectral calculation are presented in terms of averages in the following latitudinal bands:  $40^{\circ}$ - $60^{\circ}$ N,  $20^{\circ}$ - $40^{\circ}$ N,  $0$ - $20^{\circ}$ N,  $20^{\circ}$ S- $0$ ,  $40^{\circ}$ - $200$ S,  $60^{\circ}$ - $40^{\circ}$ S. Shown in Figure 2 are the spectra in the variance-preserving form, which is simply the power density multiplied by the frequency. Plotted in the linear-log form, the area under the spectra is proportional to the variance within a given frequency band. Because the repeat period of TOPEX/POSEIDON is 10 days, the shortest period of fully resolved variabilities is 20 days, although the time series was created at a 3-day interval. The longest period resolved is the annual period.

The variance at the annual period is generally higher in the northern hemisphere, reaching its maximum at  $20^{\circ}$ N- $40^{\circ}$ N. The minimum is found at the high southern latitudes  $60^{\circ}$ S- $400$ S. The simulated variance is significantly (at 95% confidence level) higher than the data in the two tropical bands ( $20^{\circ}$ S - $0$ ;  $0$ - $20^{\circ}$ N), and significantly (at 95% confidence level) lower than the data in the northern subtropical band ( $20^{\circ}$ N- $40^{\circ}$ N). (Assuming that an independent spectral estimate is made every 5 degrees by 5 degrees, the number of degrees of freedom is over 220 for the two tropical bands and 160 for the band  $20^{\circ}$ N- $40^{\circ}$ N. For a true value of unit y, 95% of the time the spectral

estimate will fall in the range of 0.87- 1.2 for the former and 0.82-1.25 for the latter, This is how the 95% confidence interval for the spectra is determined. ) The simulation and data are comparable to each other in the other 3 latitude bands. As noted above, the discrepancies are probably due to the 1000 mb wind in the tropics where the annual cycle is primarily forced by wind (Philander, 1990), and due to the inadequate vertical mixing of heat at 20°N-40°N where the annual cycle is more responsive to heat forcing (Gill and Niiler, 1973).

There is no apparent significant variance at the semiannual period in the heavily averaged spectra. The observed variance at periods shorter than the annual period is more or less evenly distributed in the intraseasonal band (20-100 days). At periods shorter than 20 days where the TOPEX/POSEIDON data have undersampled the true variance, the simulated variance is much higher than the observation outside the tropical bands, especially in the two high-latitude bands. This high variance reflects the ocean's response to the strong wind forcing by the synoptic-scale atmospheric storms. Within the two tropical bands, however, the data and simulation are basically consistent with each other with the variance of the simulation being slightly less than the data. The intraseasonal variability will be discussed in detail in Section 4.4,

[ Figure 2 near here]

#### 4.3 The annual cycle

The geographic distribution of the amplitude and phase of the annual cycle is shown in Figure 3 for both the observation and the OGCM simulation. This is only one realization of the annual cycle based on one year's worth of data. The statistical uncertainty in estimating the annual cycle per se is undoubtedly large. However, the purpose is to compare the observation to the simulation at the annual period for the particular year examined, trying to assess the model's basic performance at the annual period, instead of giving a definitive description of the phenomenon of the annual cycle.

Even based on only one year's worth of data, the annual cycle of sea level described by the

TOPEX/POSEIDON data (shown in the top panels of Figure 3) is generally in qualitative agreement with previous studies of Didden and Schott (1992) and Jacobs et al. (1992) using the Geosat data during 1987-88. (Also see Stammer and Wunsch (1994) who analyzed the same TOPEX/POSEIDON data).

[ Figure 3 near here]

Despite its somewhat stronger amplitude, the simulated annual cycle is in best agreement with the observation in the Indian Ocean, where the dynamics of the ocean's response to the dominant monsoon winds is apparently well accounted for by the model. Perigaud and Delecluse (1992) demonstrated that the sea level variability in the Indian Ocean can be well explained by a shallow-water model. It is not surprising that an OGCM does well in the Indian Ocean. Note that both the "great whirl" and its counterpart across the Arabian Sea off the west coast of the southern India are well simulated. The phase pattern between 0-20°S indicates westward annual Rossby waves (Perigaud and Delecluse, 1992).

The simulation is generally consistent with the observation in the western tropical Pacific, except for the slightly higher amplitude in the simulation. However, significant discrepancies are found in the eastern tropical Pacific, as noted in Section 4.1. Apparently the excessive upwelling in the model has resulted in a strong annual cycle along the equator, which is missing in the data. The amplitudes at 10°N and 10°S are also too strong in the simulation, so are the simulated amplitudes in the tropical Atlantic. The overall stronger amplitude in the simulation is again probably due to the 1000 mb wind forcing mentioned earlier. The phase is generally well simulated. In the tropical Pacific and Atlantic Oceans, the annual cycle of sea level is associated with a north-south seesaw pattern on two sides of the Intertropical Convergence Zone (ITCZ) located at about 7°N. Sea level anomalies north (south) of the ITCZ are positive (negative) in spring and negative (positive) in autumn. To a first-order approximation, this north-south sea level gradient is in near geostrophic balance with the eastward NECC. The NECC is strongest in autumn and weakest in spring. In some cases, the NECC completely disappeared in spring (Garzoli and Katz, 1983).

In the North Pacific and the North Atlantic, the sea level variability is mainly confined to the western boundary associated with the Kuroshio and the Gulf Stream. In general, sea level is high in autumn and low in spring. This phase pattern is well simulated by the model. However, the simulated sea level variation near the Gulf Stream tends to be more confined to the western boundary when compared with the observation. As noted earlier, it is believed that this is mainly due to the coarse horizontal resolution of the model. An eddy-resolving ocean model with  $1/6^\circ$  horizontal resolutions (Chao, unpublished manuscript, 1995) showed a much more realistic sea level variability away from the coast. Another discrepancy between the simulation and the observation is the background sea level variability in the eastern Pacific and most of the Atlantic interior. The OGCM produced only half of the seasonal sea level fluctuations in these regions. It is speculated that the subgrid-scale parameterizations are probably deficient in the model,

As indicated in the spectra shown in Figure 2, the Southern Ocean does not have much annual variability in both the data and the simulation. However, the only two regions where a strong annual cycle is observed, the Agulhas Retroflection and the Brazil/Malvinas Confluence, do not show significant amplitude in the simulation. The reason for the model's failure is probably the lack of strong nonlinearity, although improper heat forcing and mixing are also possible. Despite the weak amplitude, the phase of the annual cycle in the Southern Ocean is generally well simulated by the model.

#### 4.4 Intraseasonal variability

To reveal the spatial distribution of the intraseasonal variance shown in Figure 2, the spectral density at each location was integrated from 20 to 100 days. Shown in Figure 4 is the magnitude of the intraseasonal variability obtained this way for both the observation and the simulation. The simulation has captured most of the major spots where there is significant observed variability: the central North Pacific, the southeast Pacific, the region southwest of Australia, and the Brazil/Malvinas Confluence. In the tropics, the simulation has also reproduced the pattern of the observation. Intraseasonal oscillations in the tropical oceans have been extensively studied in

the past (Enfield and Allen, 1980; Spillane et al., 1987; Kindle and Thompson, 1989; Johns et al., 1990; Ponte and Gutzler, 1992), and are not described in the paper. The intraseasonal oscillations in the extratropical oceans, however, have not been reported extensively before, and are the main focus of this section.

[ Figure 4 near here]

Figure 5 shows the coherence between the data and the simulation estimated over the intraseasonal frequency band. Over this band, with periods from 20 to 100 days, there are 15 degrees of freedom given the 360 day record length. The level of non-zero coherence at 95% confidence level is 0.44. Only those areas with significant coherence are shown in Figure 5, which indicates that the data and the simulation are significantly correlated in time with near-zero phase lag over most of the regions where the intraseasonal variability is appreciable. Significant coherence is found even in some of the places where the level of variability is quite low: the subpolar North Atlantic Ocean, the eastern tropical Indian Ocean, the central equatorial Indian Ocean, the western subtropical Pacific Ocean, and the equatorial Pacific Ocean. Note that the overall level of variability is fairly small in this range of spatial and temporal scales, generally less than 3 cm (*rms*). The high degree of consistency between the data and simulation is reassuring for both, providing mutual validation for each in describing these weak, large-scale signals that are difficult to study using conventional in-situ measurements.

[ Figure 5 near here]

To further illustrate the consistency between the data and simulation and the spatial scales of the intraseasonal variability, Figure 6 shows the sea level time series from the data and the simulation averaged over four selected areas in the North Pacific Ocean ( $40^{\circ}\text{N}$ - $50^{\circ}\text{N}$ ,  $160^{\circ}\text{E}$ - $160^{\circ}\text{W}$ ), the southwest of Australia ( $40^{\circ}\text{S}$ - $60^{\circ}\text{S}$ ,  $80^{\circ}\text{E}$ - $120^{\circ}\text{E}$ ), the southeast Pacific Ocean ( $40^{\circ}\text{S}$ - $60^{\circ}\text{S}$ ,  $120^{\circ}\text{W}$ - $80^{\circ}\text{W}$ ), and the Brazil/Malvinas Confluence ( $40^{\circ}\text{S}$ - $50^{\circ}\text{S}$ ,  $30^{\circ}\text{W}$ - $50^{\circ}\text{W}$ ). The areas of

averaging are generally larger than 1000 km x 1000 km. In the North Pacific and South Atlantic, the annual cycle is evident. Superimposed on the annual cycle, the sea level also exhibits pronounced intraseasonal variations. In the South Indian and Pacific Oceans, intraseasonal variations dominate the time series. It is seen that the OGCM not only can reproduce the observed annual cycle, but reproduce the observed intraseasonal variations as well. The coherence between the two time series is 0.58, 0.67, 0.61, and 0.53, for the four regions noted above, respectively. All these coherence values are significantly different from zero at 95 % confidence level, indicating that the scales of these variabilities are larger than 1000 km in these regions.

[ Figure 6 near here]

It should be noted that the intraseasonal variabilities in the North Pacific and the Southern Ocean are mostly located in areas of deep abyssal plain surrounded by ridges or plateaus. For example, the major area of variability in the North Pacific is located in an area of deep abyssal plain surrounded by the Aleutian Trench to the north, the Emperor Seamounts to the west, and the Hawaiian Islands to the south. The areas of variability in the Southern Ocean are located in the Bellingshausen abyssal plain, the Weddell abyssal plain, the Enderby abyssal plain, and the South Indian abyssal plain. This suggests the potential effect of the bottom topography on the intraseasonal variations and their possible barotropic origin, which is also supported by the relatively short time scales associated with the intraseasonal variations.

There have not been sufficient in-situ observations of barotropic motions for determining their spatial distribution over the world ocean. To ascertain whether the intraseasonal sea level variations are indeed associated with barotropic motions, we calculated the rms variability of the barotropic streamfunction simulated by the OGCM, which is shown in Figure 7. Pronounced barotropic motions are found in the North Pacific Ocean and also in the Southern Ocean. These regions of strong barotropic motions coincide with those regions of strong intraseasonal variations as shown in Figure 5. Shown in Figure 8 is the coherence between the barotropic stream function and the simulated sea level averaged over the intraseasonal frequencies, indicating that the

intraseasonal sea level variations at the high latitudes are indeed associated with barotropic motions. These barotropic motions are primarily forced by the large-scale wind stress curl (FLI and Davidson, 1995). The high degree of coherence between the observation and simulation also validates to some extent the quality of the NMC winds used to drive the model. This is somewhat surprising in the high-latitude Southern Ocean,

The results from the present study is consistent with the previous findings of Niiler and Koblinsky (1985) and Koblinsky et al. (1989), suggesting strong barotropic oceanic response to wind forcing in the North Pacific Ocean at the intraseasonal time scales. Moreover, the present study has provided a global distribution of the regions where barotropic response of the ocean to wind forcing is expected.

[ Figure 7 and Figure 8 near here]

## 5 Summary and discussions

The TOPEX/POSEIDON altimetric sea level observation during 1992-93 was used to validate the simulation by a version of the Modular Ocean Model forced by the daily wind stress and heat flux derived from the NMC 1000-mb operational analysis. The model simulation was compared to the observation at spatial scales on the order of 500 km and larger. Only the temporal variations are examined. The model is able to explain a significant amount of the variance of the data, which is composed primarily of the annual cycle and intraseasonal fluctuations (periods shorter than 100 days). At periods longer than 20 days, which is the Nyquist period of the TOPEX/POSEIDON sampling scheme, the annual cycle generally dominates the variance north of 20°S, south of which the variance is somewhat evenly distributed across all the frequencies.

The basic features of the annual cycle are simulated well by the model. Major discrepancies are found in the eastern tropical Pacific, where the simulated annual cycle is too strong and the spatial pattern is more complex than the observation. It is suspected that the upwelling in the model is too strong in the region and creates the erroneous annual cycle (Stockdale et al., 1993).

Moreover, the simulated annual cycle is too weak in the eastern North Pacific and most of the interior of the North Atlantic. This is probably due to the model deficiency in parametering the subgrid scale processes, Another possible error in the model comes from the heat and fresh-water fluxes. Although the sensible and latent heat fluxes are calculated through the bulk formula using the NMC real-time operational analysis, the short-wave and long-wave radiation fluxes are assumed to be the annual-mean values, and are only a function of latitude. This can be improved by using the climatological radiation fluxes, e.g., the Comprehensive Ocean-Atmosphere Data Sets (COADS, De Silva et al., 1995). Although the fresh-water flux is not available during the TOPEX/POSEIDON period, the climatological fresh-water flux is available (Oberhuber, 1988), and should be used in the future.

Another improvement in the model simulation can be made by increasing the spatial resolution in both horizontal and vertical directions. The current model with 2 degrees in longitude and 1 degree in latitude fails to simulate the Gulf Stream at the right place. As a result, the simulated sea level variability is more confined to the coastal boundary than the data suggests. A recent modeling study with eddy-resolving resolutions (1/6 degree) over the North Atlantic Ocean is able to simulate the Gulf Stream at the right place, and therefore produce the right sea level variability associated with the Gulf Stream (Chao, unpublished manuscript, 1995).

Significant intraseasonal variability is found in the central North Pacific and the Southern Ocean. The simulation is highly correlated with the observation at periods from 20 to 100 days. The spatial scales are larger than 1000 km in many places. Comparison of the simulated sea level variations to the model barotropic streamfunction suggests that these variabilities are apparently the barotropic response of the ocean to wind forcing. Due to the large spatial scales and short temporal scales of these variabilities, they have been difficult to study using in-situ observations. The present study provides evidence for the global distribution of these variabilities and the model's capability of describing them. The global distribution of the barotropic motions revealed by the study (Figure 4) can be used by sea-going oceanographers who can strategically deploy current meters in the deep ocean and study the dynamical relationship between the wind and deep ocean currents.

The dynamics of these intraseasonal variations still remain to be determined. The

atmospheric zonal wind stress, which is used to drive the model, does contain strong intraseasonal fluctuations (not shown here). Using the TOPEX/POSEIDON data and the NMC wind stress, Fu and Davidson (1995) found marginal but significant correlation between the atmospheric wind curl and the linear oceanic barotropic vorticity in the North and South Pacific Ocean. Their results and the present study suggest that some of the intraseasonal sea level fluctuations cannot be explained by the linear barotropic response to the atmospheric wind forcing alone (such as the South Indian Ocean and South Atlantic Ocean). Work is currently underway to study the nonlinear aspect of the oceanic response to the atmospheric wind stress. Most of the variabilities in the southern Ocean occur in regions of closed  $f/H$  ( $f$  is the Coriolis parameter,  $H$  the depth of the ocean) contours, suggesting possible near-resonant response of the ocean (Leipold, 1983; Koblinsky, 1990). One would also wonder about the relationship between these intraseasonal variations in the extratropical oceans and those in the tropics as described in the previous studies (Enfield and Allen, 1980; Spillane et al., 1987; Kindle and Thompson, 1989; Johns et al., 1990; Ponte and Gutzler, 1992).

The present study basically suggests that the large-scale, adiabatic wind-driven dynamics of the ocean are probably well represented in the model, as evidenced by the model's success in simulating the variabilities of the Indian Ocean and the extratropical intraseasonal variabilities. However, the excessive energy in the simulation indicates the possible errors in the wind forcing. As noted above, the discrepancies in the model's simulation of the annual cycle in the eastern tropical Pacific and the interiors of the northern mid-latitude oceans reveal possible deficiencies in the model's thermohaline forcing and mixing parameterizations. It is anticipated that assimilation of the altimeter data into the model would mitigate these model deficiencies and improve the model's ability in describing the 3-dimensional state of the ocean (at least in the upper ocean above the main thermocline). Such an effort is underway.

## Acknowledgements

The research described in this publication was carried out by the Jet Propulsion Laboratory (JPL), California Institute of Technology, under a contract with the National Aeronautics and Space Administration (NASA). This work is also supported by the JPL Director Discretionary Fund and the TOPEX/POSEIDON project under an Announcement of Opportunity. Computations were performed at NASA JPL and NASA Ames Research Center Numerical Aerodynamics Simulation facilities through the JPL Supercomputing Project. We are grateful to National Ocean and Atmosphere Administration (NOAA) Geophysical Fluid Dynamics Laboratory (GFDL) for providing the Modular Ocean Model. We acknowledge Greg Pihos for providing the gridded TOPEX/POSEIDON data, and Wendy Tang for providing the NMC operational analysis. Comments from Greg Jacobs and another anonymous reviewer greatly help to improve the original manuscript. Conversations with Roger Davidson, Ichiro Fukumori, Claire Perigaud, Ramanujam Raghunath, Victor Zlotnicki during the course of this work are also acknowledged.

## References

- Blayo, E., J. Verron, and J. M. Molines, Assimilation of TOPEX/POSEIDON altimeter data into a circulation model of the North Atlantic, *J. Geophys. Res.*, 99, 24,691-24,705, 1994.
- Bryan, K., A numerical method for the study of the world ocean circulation, *J. Comput. Phys.*, 4, 1687-1712, 1969,
- Callahan, P. TOPEX/POSEIDON Project GDR Users Handbook, JPL 1)-8944 (internal document), Jet Propulsion Laboratory, Pasadena, Calif., 84pp, 1993.
- Cartwright, D. E., and R. D. Ray, Oceanic tides from Geosat altimetry, *J. Geophys. Res.*, 95, 3069-3090, 1990.
- Chao, Y., and S. G. H. Philander, On the structure of the Southern Oscillation, *J. Climate*, 6, 450-469, 1993.
- Chao, Y., D. Halpern, and C. Perigaud, Sea surface height variability during 1986-1988 in the tropical Pacific Ocean, *J. Geophys. Res.*, 98, 6947-6959, 1993.
- Cox, M. D., A primitive equation, 3-dimensional model of the ocean, Ocean Group Tech. rep. 2, 143pp, Geophysical Fluid Dyn. Lab., Princeton, N. J., 1984.
- deSilva, A. M., C. C. Young, and S. Levitus, Atlas of surface marine data 1994, Vol. 1: Algorithms and procedures, Data Assimilation Office, NASA Tech. Rep., 74pp, 1994.
- Didden, N., and F. Schott, Seasonal variations in the western tropical Atlantic: surface circulation from Geosat altimetry and WOCE model results, *J. Geophys. Res.*, 97,3529-3541, 1992.
- Enfield, D. B., and J. S. Allen, On the structure and dynamics of monthly mean sea level anomalies along the Pacific coast of North and South America, *J. Phys. Oceanogr.*, 10, 557-578, 1980.
- Fu, L.-L., E. J. Christensen, C. A. Yamarone, Jr., M. Lefebvre, Y. Menard, M. Dorrer, and P. Escudier, TOPEX/POSEIDON mission overview, *J. Geophys. Res.*, 99,24,369-24,381, 1994.
- Fu, L.-L., and G. Pihos, Determining the response, of sea level to atmospheric pressure forcing using TOPEX/POSEIDON data, *J. Geophys. Res.*, 99, 24,633-24,642, 1994.

- Fu, L.-L., and R. Davidson, A note on the barotropic response of sea level to time-dependent wind forcing, *J. Geophys. Res.*, (accepted), 1995.
- Garzoli, S. L., and E. J. Katz, The forced annual reversal of the Atlantic North Equatorial Countercurrent, *J. Phys. Oceanogr.*, **13**, 2082-2090, 1983.
- Ghil, M., and P. Malanotte-Rizzoli, Data assimilation in meteorology and oceanography, *Adv. Geophys.*, **33**, 141-266, 1991.
- Gill, A. E., and P. Niiler, Theory of seasonal variability in the ocean, *Deep-Sea Res.*, **20**, 141-177, 1973.
- Hellerman, S., and M. Rosenstein, Normal monthly wind stress over the world ocean with error estimates, *J. Phys. Oceanogr.*, **13**, 1093-1104, 1983.
- Jacobs, G. A., G. H. Born, M. E. Parke, and P. C. Allen, 'The global structure of the annual and semi-annual sea surface height variability from Geosat altimeter data, *J. Geophys. Res.*, **97**, 17,813-17,828, 1992.
- Johns, W. E., T. N. Lee, F. A. Schott, R. J. Zantopp, and R. H. Evans, 'The North Brazil Current Retroflection: Seasonal structure and eddy variability, *J. Geophys. Res.*, **95**, 22,103-22,120, 1990.
- Kindle, J. C., and J. D. Thompson, The 26- and 50-day oscillations in the western Indian Ocean: Model results, *J. Geophys. Res.*, **94**, 4721-4736, 1989.
- Koblinsky, C. J., P. Niiler, and W. J. Schmitz, Jr., Observations of wind-forced deep ocean currents in the north Pacific, *J. Geophys. Res.*, **94**, 10,773-10,790, 1989.
- Koblinsky, C., The global distribution of  $f/H$  and the barotropic response of the ocean, *J. Geophys. Res.*, **95**, 3213-3218, 1990.
- Leetmaa, A., and M. Ji, Operational hindcasting of the tropical Pacific, *Dyn. Atmos. Oceans*, **13**, 465-490, 1989.
- Leipold, G., Vorticity oscillations over closed- $f/H$  contours, Hamburg. *Geophys. Einzelschr.*, 94pp, 1983.
- Levitus, S., Climatological atlas of the world ocean, Prof. Pap. 13, 173pp, Natl. Oceanic and Atmos.

- Admin., Silver Spring, Md., 1982.
- Ly, L. N., J. C. Kindle, J. D. Thompson, and W. J. Youtsey, Wind stress analysis over the western equatorial Pacific and North Atlantic Oceans based on ECMWF operational wind products, Institute of Naval Oceanography Tech. Rep., 109pp, 1992.
- Mellor, G. L., and T. Yamada, Development of a turbulence closure model for geophysical fluid problems, *Rev., Geophys. Space Phys.*, 20, 851-875, 1982
- Mitchum, G., Comparison of TOPEX sea surface heights and tide gauge sea levels, *J. Geophys. Res.*, 99,24,541-24,554, 1994.
- Nerem, R. S., E. J. Schrama, C. J. Koblinsky, and B. D. Beckley, A preliminary evaluation of ocean topography from the TOPEX/POSEIDON mission, *J. Geophys. Res.*, 99, 24,565-24,583, 1994.
- Niiler, P., and C. J. Koblinsky, A local time dependent Sverdrup balance in the northeastern Pacific, *Science*, 229,754-756, 1985.
- Oberbuber, J. M., An atlas based on the COADS data set: The budget of heat, buoyancy and turbulent kinetic energy at the surface of the global ocean, Max-Planck-Institut für Meteorologic, Hamburg, Germany, 100pp, 1988.
- Pacanowski, R., and S. G. H. Philander, Parameterization of vertical mixing in numerical models of tropical oceans, *J. Phys. Oceanogr.*, 11, 1443-1451, 1981.
- Pacanowski, R., K. Dixon, and A. Rosati, **Modular Ocean Model Users Guide**, Ocean Group Tech. Rep. 2, Geophysical Fluid Dyn. Lab., Princeton, N. J., 1991.
- Perigaud, C., and P. Delecluse, Annual sea level variations in the tropical Indian Ocean from Geosat and shallow-water simulations, *J. Geophys. Res.*, 27, 20,169-20,179, 1992.
- Philander, S. G. H., El Niño, La Niña and the Southern Oscillation, Academic Press, 283pp, 1990.
- Ponte, R. M., and D. S. Gutzler, 40-60 day oscillations in the western tropical Pacific: Results from an eddy-resolving global ocean mode,], *Geophys. Res. Lett.*, 19, 1475-1478, 1992.
- Rosati, A., and K. Miyakoda, A general circulation model for upper ocean simulation, *J. Phys. Oceanogr.*, 18, 1601-1626, 1988.

- Schrama, E. J. O., and R. D. Ray, A preliminary tidal analysis of TOPEX/POSEIDON altimetry, *J. Geophys. Res.*, 99,24,799-24,808, 1 994.
- Spillane, M. C., and D. B. Enfield, and J. S. Allen, Intraseasonal oscillations in sea level along the west coast of the Americas, *J. Phys. Oceanogr.*, **17**, 313-325.
- Stammer, D., and C. Wunsch, Preliminary assessment of the accuracy and precision of TOPEX/POSEIDON altimeter data with respect to the large-scale ocean circulation, *J. Geophys. Res.*, 99,24,584-24,604, 1994.
- Stockdale, T., D. Anderson, M. Davey, P. Delecluse, A. Kattenberg, Y. Kitamura, M. Latif, and T. Yamagata, Intercomparison of tropical ocean GCMs, WMO/TD-No.545, 43pp, 1993.
- Wu, J., Wind-stress coefficients over sea surface from breeze. to hurricane, *J. Geophys. Res.*, 87, 9704-9706, 1982.
- Wunsch, C., Bermuda sea level in relation to tides, weather, and baroclinic fluctuations, *Rev. Geophys.*, 1 ( ), 1-49, 1972.

## Figure captions

Figure 1 Root-Mean-Square (RMS) variability of sea surface height derived from the TOPEX/POSEIDON data and the OGCM simulation.

Figure 2 Power spectra of sea level derived from the TOPEX/POSEIDON data (solid) and the OGCM simulation (dot) averaged over six latitudinal bands:  $40^{\circ}$ - $60^{\circ}$ N,  $20^{\circ}$ - $40^{\circ}$ N,  $0$ - $20^{\circ}$ N,  $20^{\circ}$ S- $0$ ,  $40^{\circ}$ - $200$ S,  $60^{\circ}$ - $400$ S.

Figure 3 The amplitude and phase of the annual cycle derived from the TOPEX/POSEIDON data and the OGCM simulation.

Figure 4 The amplitude and phase of the intraseasonal oscillations (with periods from 20 to 100 days) derived from the TOPEX/POSEIDON data and the OGCM simulation.

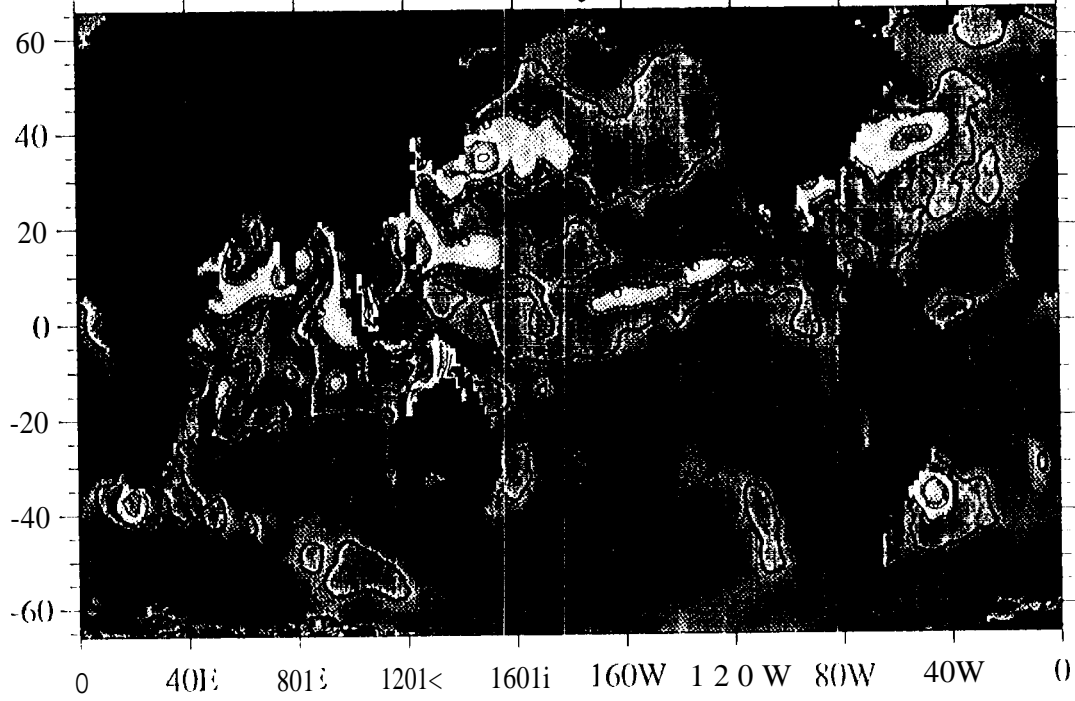
Figure 5 The amplitude and phase of the coherence between the TOPEX/POSEIDON data and the OGCM simulation averaged over the intraseasonal frequencies with periods from 20 to 100 days.

Figure 6 The sea level time series from the TOPEX/POSEIDON data and the OGCM simulation averaged over areas in the North Pacific Ocean ( $40^{\circ}$ N- $50^{\circ}$ N,  $160^{\circ}$ E- $160^{\circ}$ W), the southeast Indian Ocean ( $40^{\circ}$ S- $600$ S,  $80^{\circ}$ E- $120^{\circ}$ E), the southeast Pacific Ocean ( $40^{\circ}$ S- $600$ S,  $120^{\circ}$ W- $80^{\circ}$ W), and the southwest Atlantic Ocean ( $40^{\circ}$ S- $500$ S,  $30^{\circ}$ W- $50^{\circ}$ W).

Figure 7 Root-Mean-Square (RMS) variability of the OGCM-simulated barotropic streamfunction.

Figure 8 The amplitude of the coherence between the OGCM-simulated sea level and barotropic streamfunction averaged over the intraseasonal frequencies with periods from 20 to 100 days.

Sea Level RMS Variability (TOPEX/POSEIDON)



Sea Level RMS Variability (OGCM)

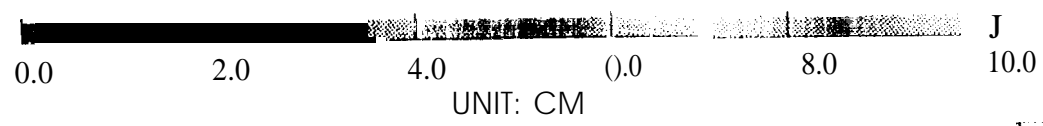
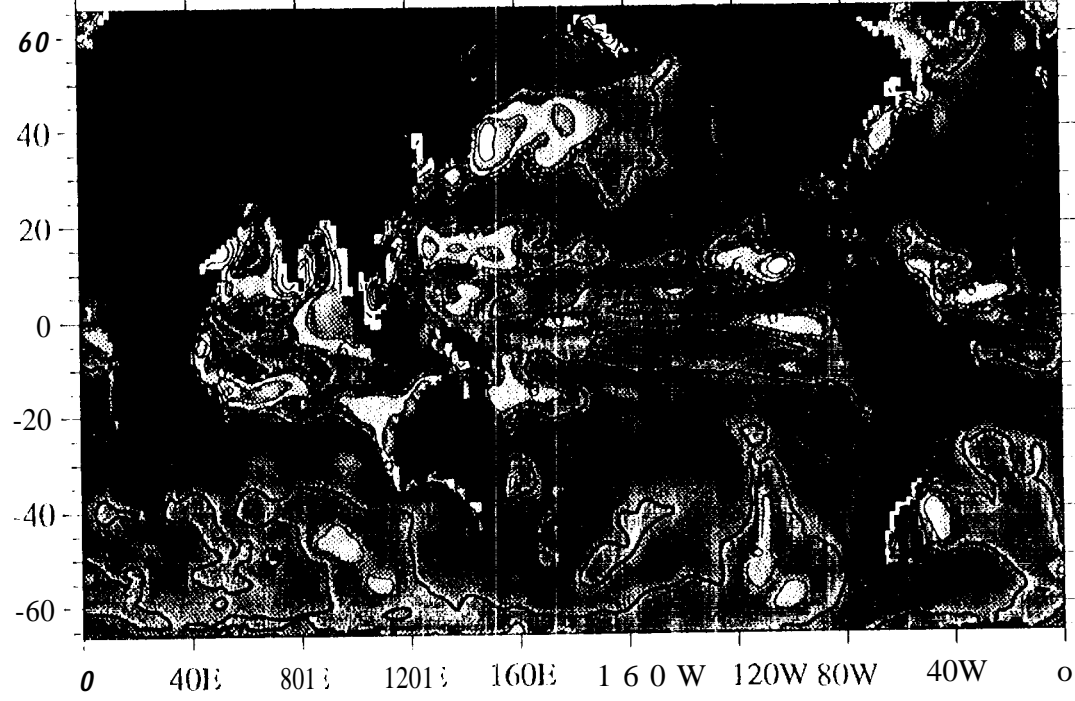


Fig. 1

Power Spectral Density \* Frequency (cm<sup>2</sup>)

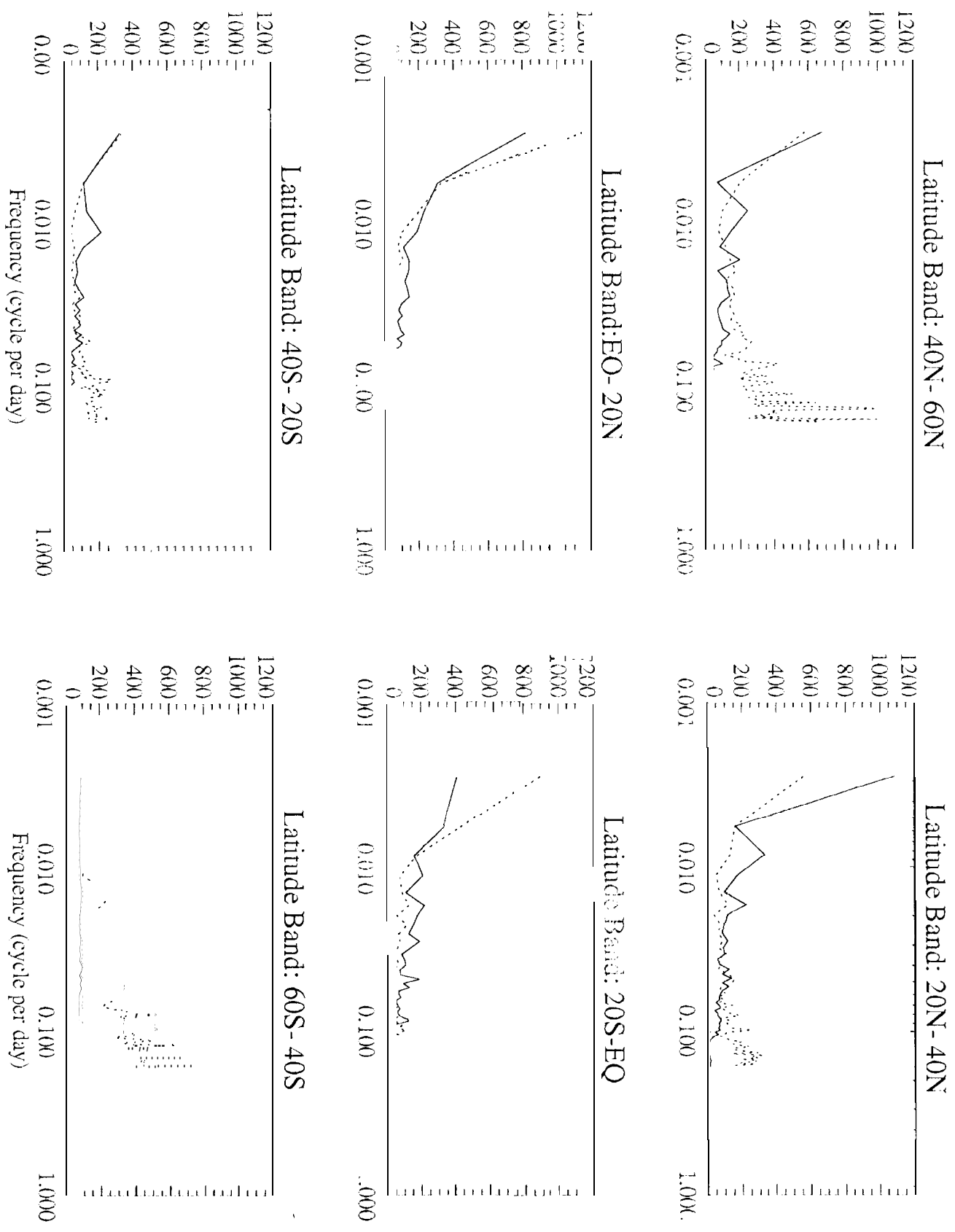
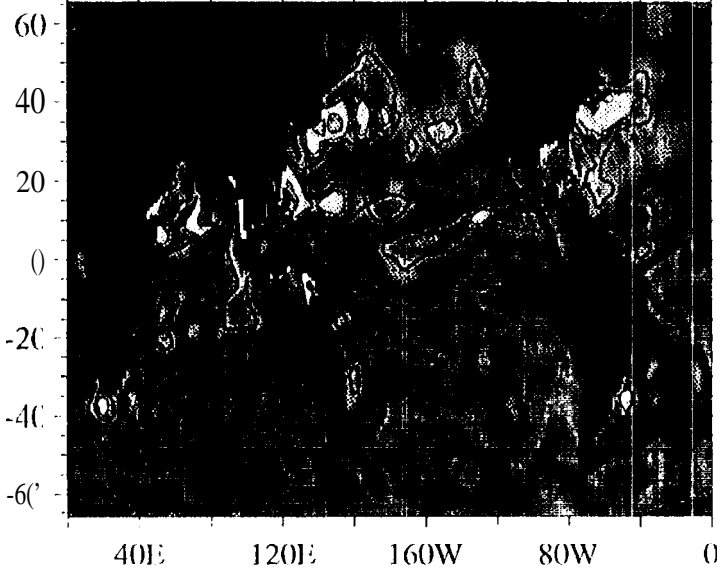
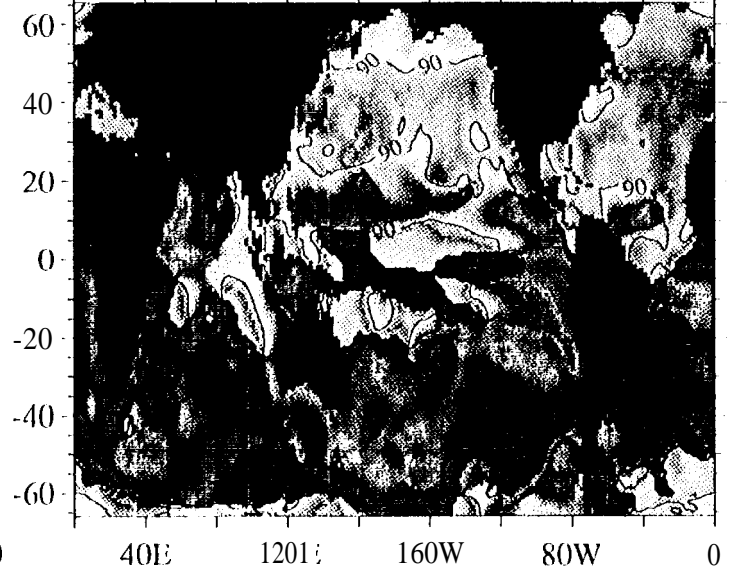


Fig 2

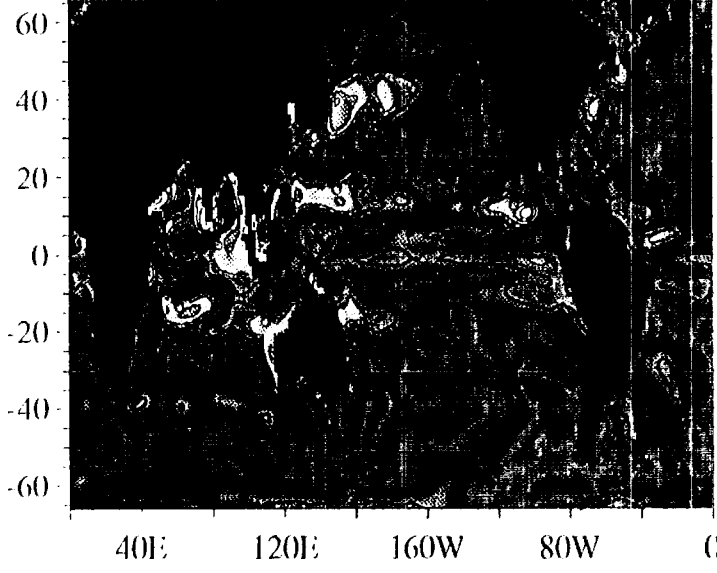
Annual Amplitude (TOPEX/POSEIDON)



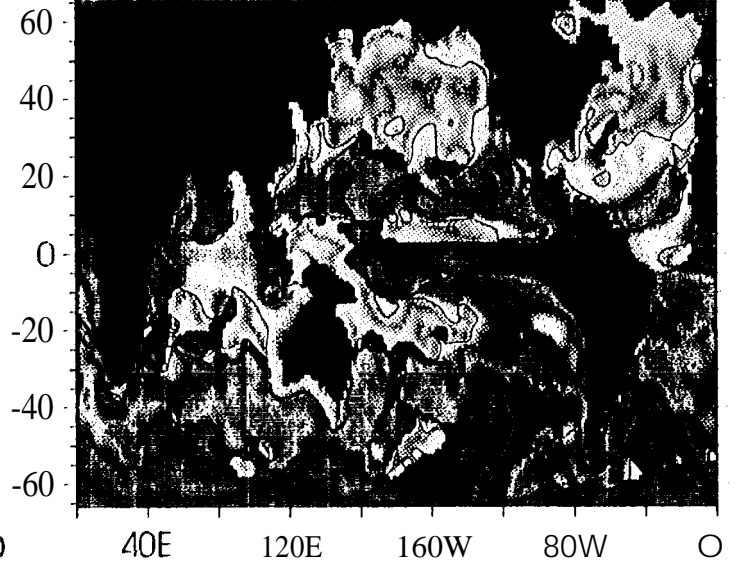
Annual Phase (TOPEX/POSEIDON)



Annual Amplitude (OGCM)



Annual Phase (OGCM)



2.0 4.0 6.0 8.0  
UNIT: CM

-90.0 0.0 90.0  
UNIT: degree

Fig 3

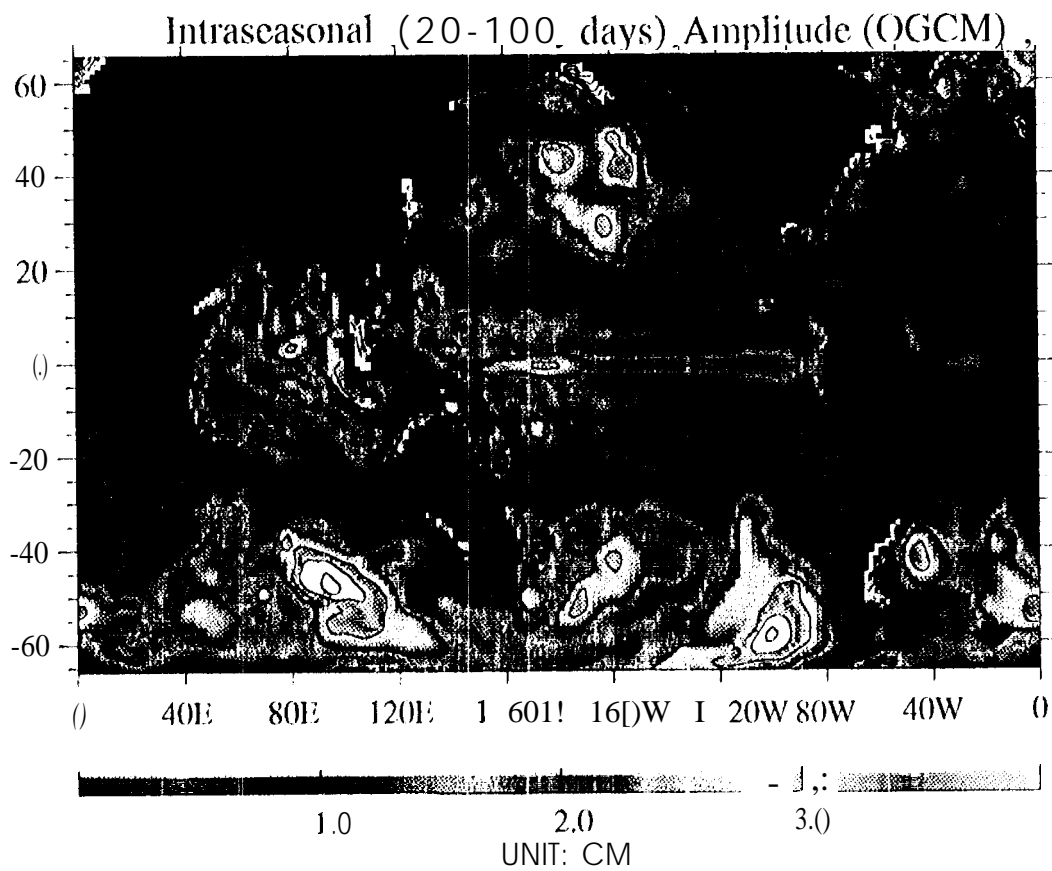
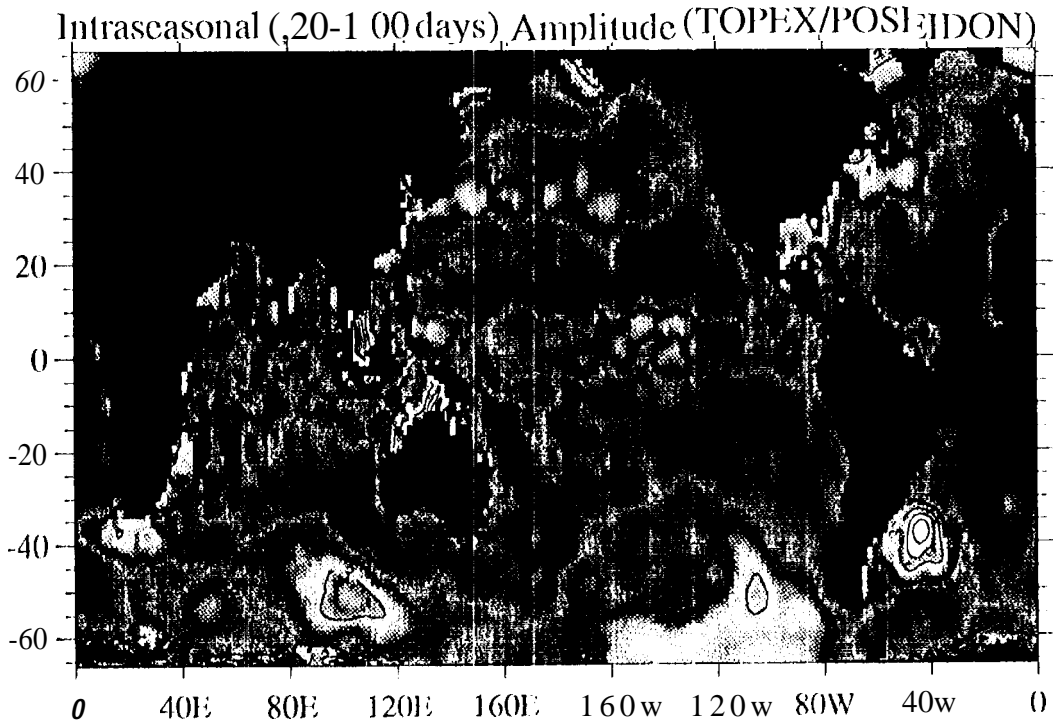


Fig. 4

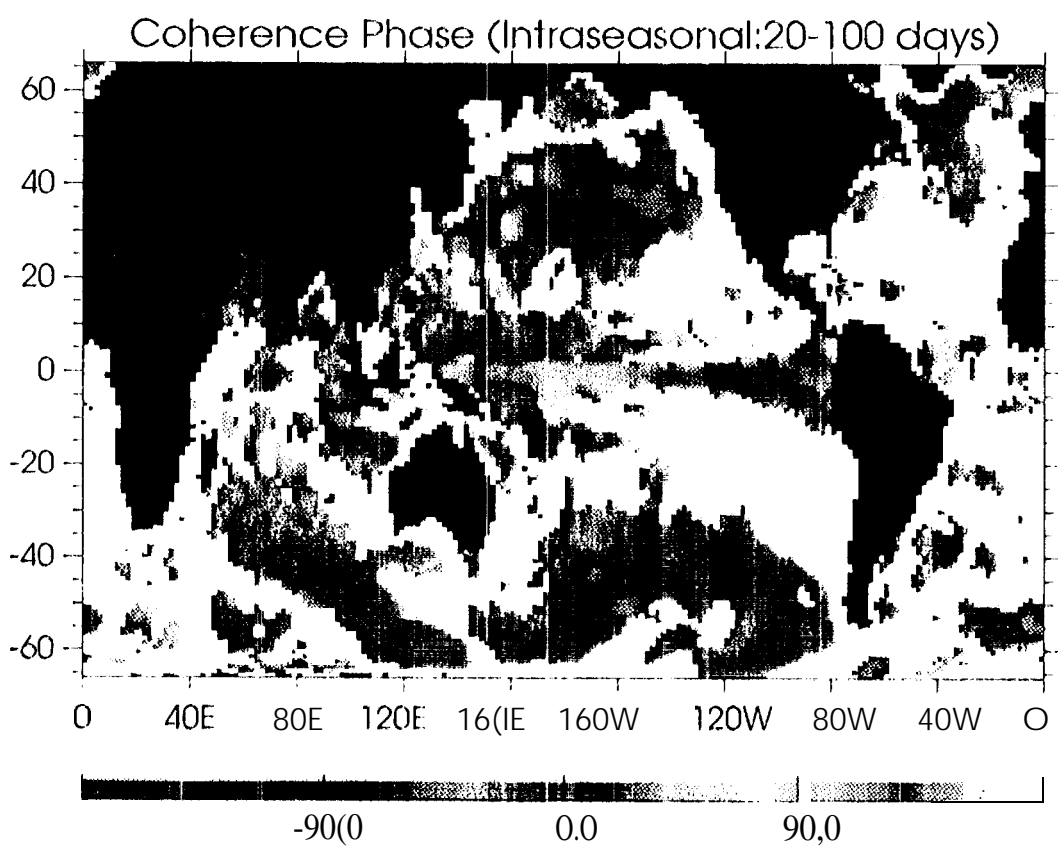
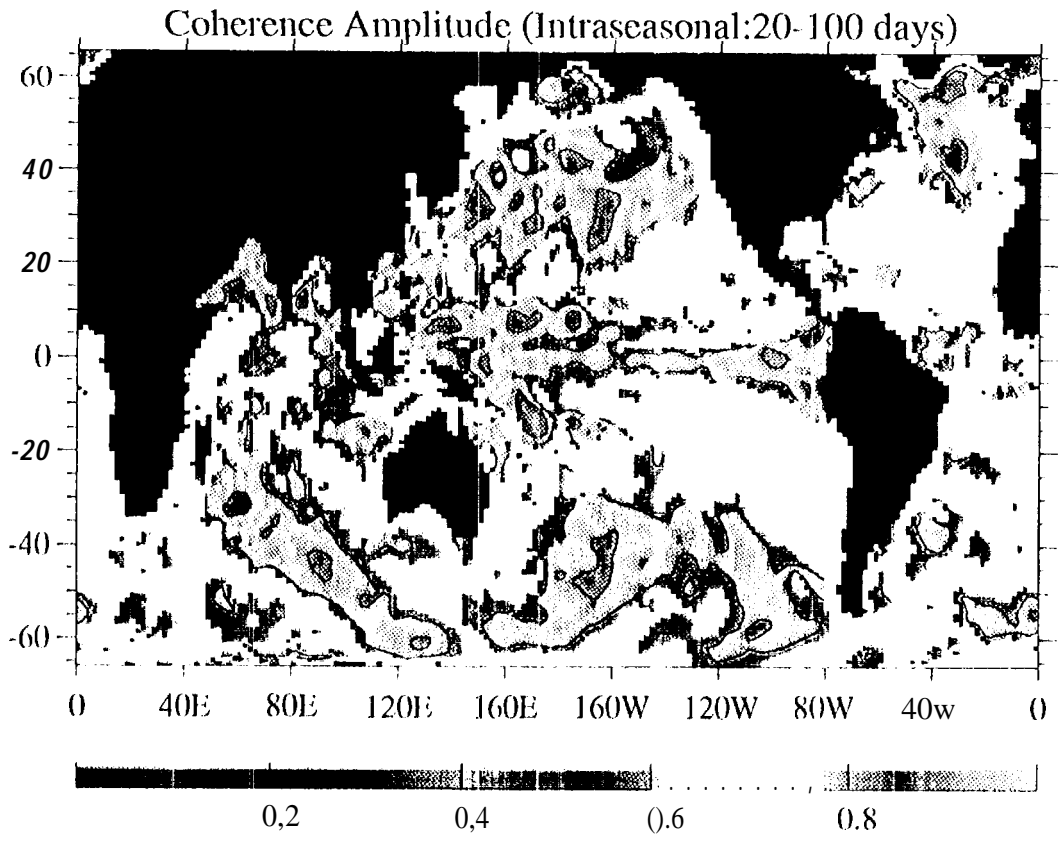
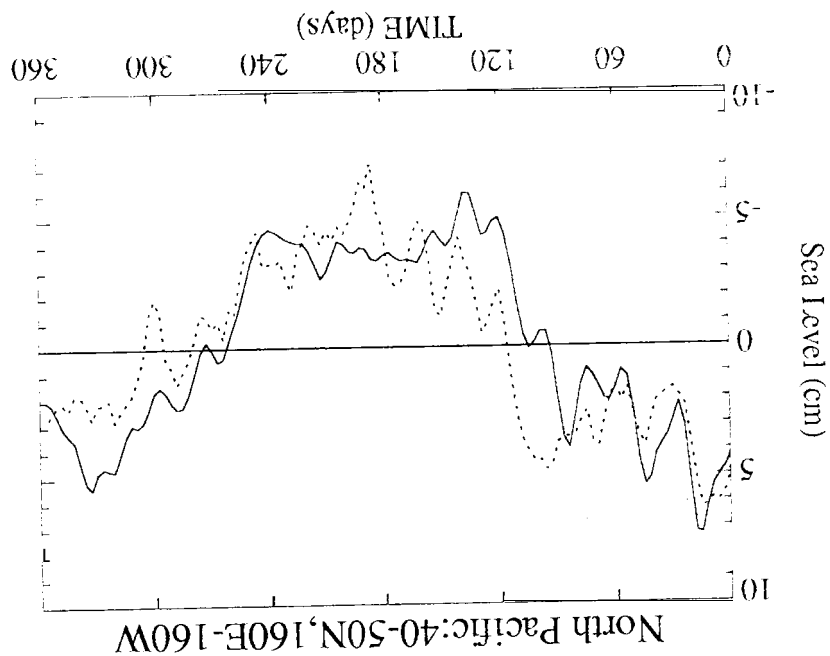
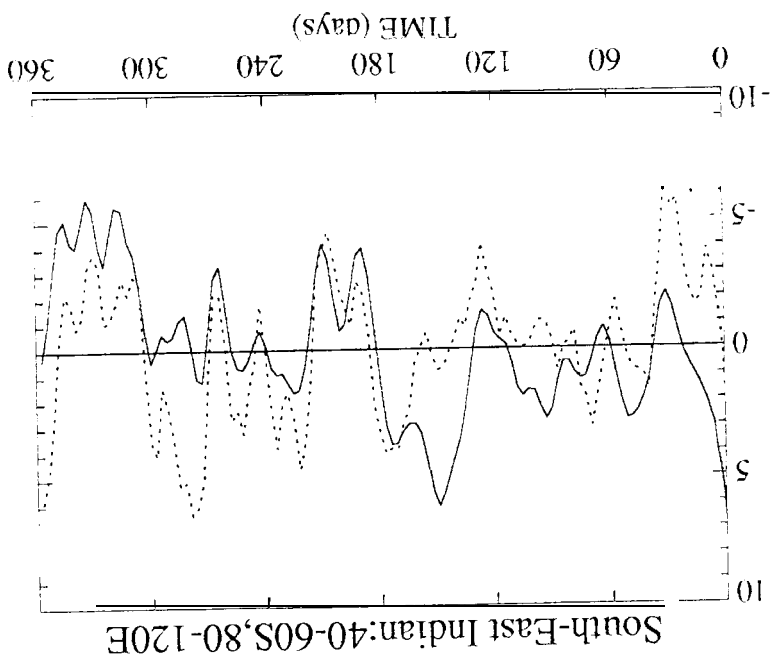
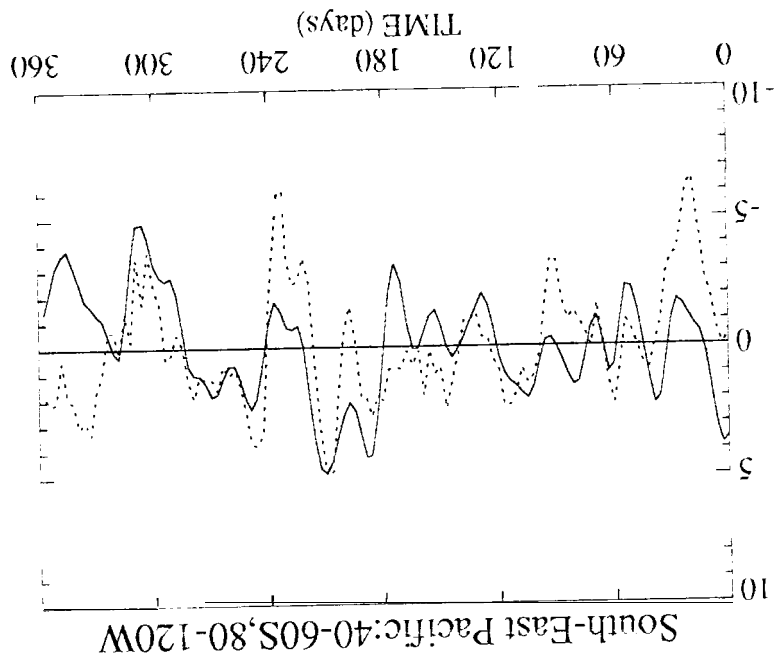
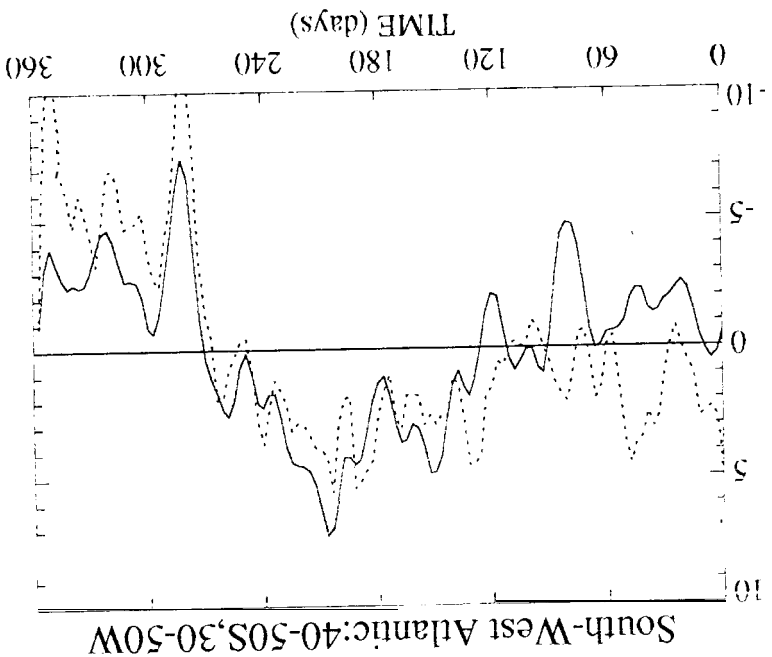


Fig. 5

Fig. 6



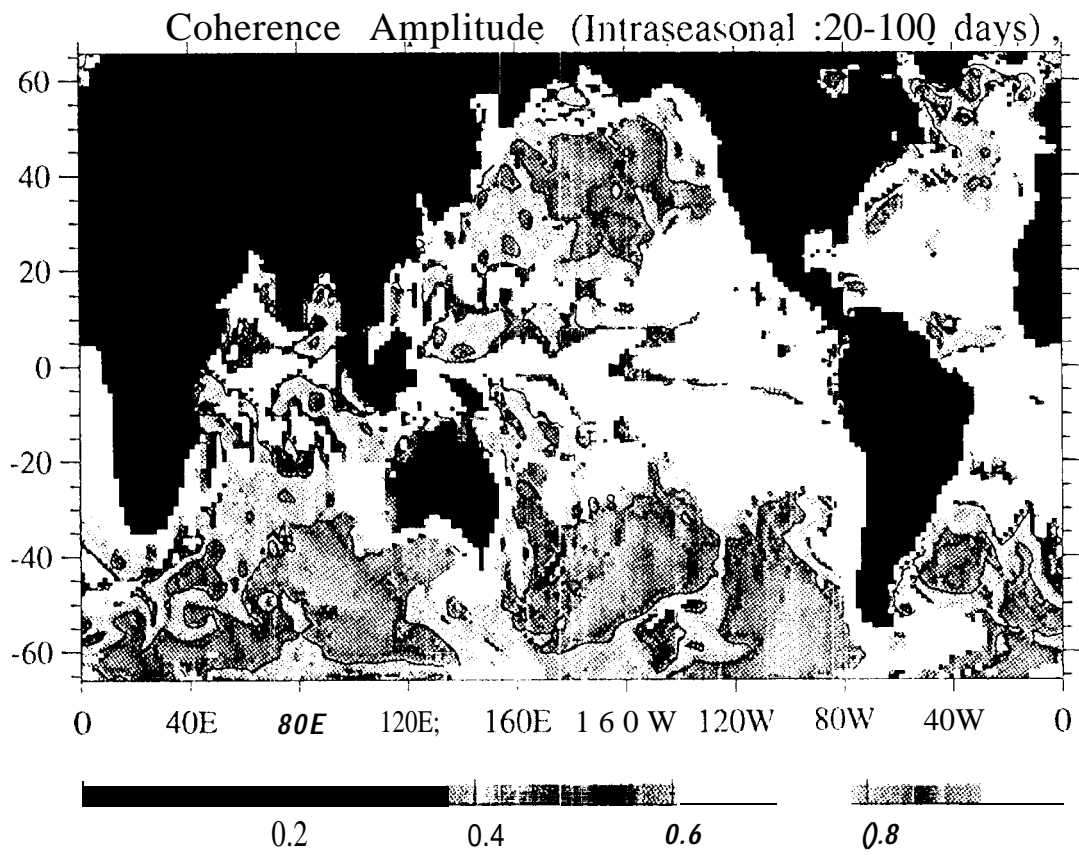


Fig. 8